

# Microstructural characterisation and hardness of Fe-Mn alloys compared to commercial 9%Nickel alloy

*Lebedike Mampuru*<sup>1,2</sup>, *Maje Phasha*<sup>1</sup>, *Michael Bodunrin*<sup>2</sup>, *Desmond Klenam*<sup>2</sup> and *Joseph Moema*<sup>1</sup>

<sup>1</sup> Advanced Materials Division, MINTEK, South Africa,

<sup>2</sup> Faculty of Engineering and the Built Environment, School of Chemical and Metallurgy, University of Witwatersrand, Johannesburg

[lebidikem@mintek.co.za](mailto:lebidikem@mintek.co.za), [majep@mintek.co.za](mailto:majep@mintek.co.za), [michael.bodunrin@wits.ac.za](mailto:michael.bodunrin@wits.ac.za),  
[desmond.kleman@wits.ac.za](mailto:desmond.kleman@wits.ac.za), [josephm@mintek.co.za](mailto:josephm@mintek.co.za)

**Abstract.** Increased energy demand globally due to population growth opens opportunities for alternative energy sources. Liquefied natural gas is gaining traction as an alternative to diversifying energy supply. 9%Nickel steel is used in the construction of tanks for storage and transportation of liquefied natural gas because of its high toughness and tensile strength properties. This alloy is not readily available because of its complex production process and high cost. In this research, cast Fe-Mn-based alloys are explored as an alternative to 9%Nickel steel. Computer-simulated binary compositions are cast and subjected to a thermomechanical process. Thermomechanically processed alloys are microstructurally assessed and harness tested as the initial evaluation step in selecting high-performing base alloy for further alloying. Alloy.

## 1 Introduction

The constraints imposed by energy deficiencies stemming from breakdowns in power generation equipment, coupled with heightened demands due to population expansion and economic advancement, afford prospects for alternative energy sourcing [1, 2]. Among these alternatives, liquefied natural gas (LNG) has garnered considerable attention as a viable option for diversifying the energy mix. However, the storage and transportation of LNG require engineered and specialised alloyed materials with robust structural integrity under cryogenic conditions. A typical example is the commercial 9%Nickel steel alloy. This alloy is used mainly for the construction of tanks, pipelines, and structural components for the storage and transportation of LNG. Its adoption is based on its commendable toughness and tensile strength under ambient and cryogenic temperatures [1–4]. Although an alloy of choice, there are drawbacks such as high costs due to the alloying elements and specialized processes associated with manufacturing. Hence, a need to explore alternative low-cost Fe-based structural steels.

The Fe-Mn-based alloys are promising alternatives. They are cost-effective due to the low-cost alloying elements of Mn and Fe, and also lighter than the 9 wt% Ni-based alloys. The Mn contents contribute to toughness which can be explored in the cryogenic temperature domain. Mn is also an austenite phase stabiliser. This can substitute Ni which is expensive. The Fe content contributes to strength which is critical for load-bearing or structural applications. The drive for Fe-Mn structural steels provides the opportunity for value addition and the mineral beneficiation strategy of South Africa. Currently, South Africa has ~77% of the global reserves of Mn [5] hence developing structural and functional materials is essential for the downstream economic expansion.

This paper focuses on microstructural property assessment and characterisation as well as hardness evaluation of produced and thermomechanically processed Fe-Mn binary alloys in comparison to commercial 9%Ni alloys. This evaluation is for benchmarking the amount of manganese in the base alloy for improved toughness properties on further alloying. The underlying microstructure interactions and toughening mechanisms are established before exploring the implications of the current results for the design of robust ferrous alloys for the storage of liquefied natural gas.

## 2 Methodology

### 2.1 Materials casting and rolling

Two binary Fe-Mn compositions (A1 and A2) and 9%Ni steel alloy (Reference) listed in Table 1 below, were cast in the form of ingots using a 50kg medium frequency induction furnace. The induction furnace was fitted with an alumina cast crucible which was backfilled with MR21 refractory material. The crucible was installed and baked for a few hours before the casting to remove any moisture, which would be deleterious to the casting process. The ingots were cast into an open silica gel bonded sand mould. Their dimensions were (length by thickness) 260mm x 45mm, a representative sample is shown in Figure 1. Casting was done in the open air. The produced ingots were then sectioned as indicated by the black line in Figure 1. One part (bottom) was taken for further study.

As-cast specimens were sectioned from each ingot as indicated by the red square (in Figure 1) and then the remaining ingot was taken for thermomechanical processing. The blue line illustrates the rolling direction of the ingot and the red arrow indicates the side to be analysed which is parallel to the processing/rolling direction. Rolling was conducted as per the schedule shown in Figure 2. The rolling was done on 45mm thick ingots to 12.5mm plates as per the parameters in Table 2. The ingots were heated to 1200°C in a muffle furnace and held for 2 hours, then rolled from 45mm through to 21mm and returned to the furnace for 20 minutes. After 20 minutes of soaking, they were rolled down to 12.5mm gauge for three passes then water quenched. Figure 3, shows a representative image of the ingots after rolling. Specimens were also sectioned from each hot rolled (HR) plate using a CNC wire cutter fitted with a 0.25mm molybdenum wire. The microstructure and mechanical properties such as hardness, were conducted and results are discussed.

**Table 1.** Chemical composition of the two binary FeMn compositions and 9% Ni alloy.

Alloy Name	Chemical Composition wt%						
	C	Si	Mn	S	P	Ni	Fe
Reference	0.13 max	0.13 - 0.45	0.98	0.015	0.015	9.6	Remainder
A1	-	-	19 - 22	-	-	-	78 - 81
A2	-	-	22 - 25	-	-	-	75 - 78



**Fig. 1.** A representative ingot in the as-cast condition showing the sectioned areas and the rolling direction.

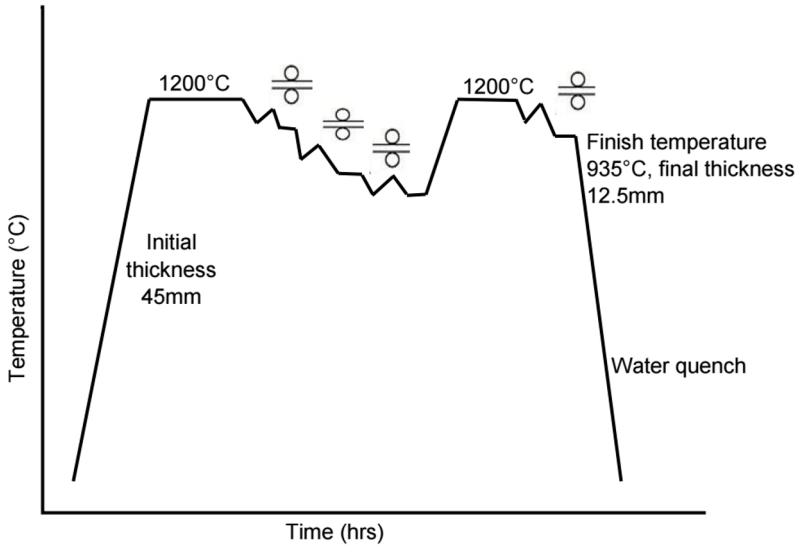


**Fig. 2.** The thermomechanical processing schedule schematic for hot rolling of the ingots.

**Table 2.** The parameters for thermomechanical processing of the ingots.

No. Passes	Temp.(°C)	Sample Thickness (Before pass) (mm)	Sample Thickness (After Pass) (mm)	Reduction (mm)	Strain (%)
1x pass	1200	45	35	10	23
1 x pass	990	35	27	8	
1x pass	867	27	21	6	
3x Pass	1200	21	12.5	8.5	40



**Fig. 3.** A representative image showing the ingots after the rolling schedule.

## 2.2 Analytical procedures and equipment used

Specimens from each of the alloys ingots including the reference, in the as-cast and rolled condition, were ground from 120 grit, 400 grit, 800 grit and 1200 grit then polished from 6micron, 3micron and 1micron finish. All the above steps were done using a Struers abrapol20 polisher with a force of 150N at the speed of 300RPM. Optical microscopy (OM) and X-ray diffraction (XRD) were used for microstructural and phase analysis. To reveal the general microstructures of the specimens, 5% Nital was used as an etchant. Olympus DSX 510 light microscope was used for analysis. Vickers hardness was done on the specimen using an EMCO hardness machine and a load of 10kgF. The phase constitutions of the Fe–Mn and Reference alloy specimens were identified by Bruker D8 advance XRD machine using Co–K $\alpha$  radiation, recorded in the  $2\theta$  range from  $0^\circ$  to  $90^\circ$ .

## 3 Results and discussion

### 3.1 Microstructure and XRD

The specimens of the cast Fe-Mn (A1 and A2) and 9%Ni alloys were subjected to microstructural analysis and hardness tests and the observed properties results were compared to the literature.

The as-cast microstructure of the Reference (Figure 4, left) is shown together with the A1 (Figure 4, right) and A2 (Figure 4, bottom). The microstructure of the reference appears martensitic (brown) with patches of retained austenite (lighter areas), which is critical for this composition as it contributes to the toughness required in use at subzero temperatures [4]. The amount of Ni (about 9%) added suppresses the formation of high-temp transformation phases such as ferrite and pearlite [4]. XRD phase analysis scans for this reference showed BCC as the major structure, see Figure 5. The A1 and A2 microstructures were typical of a high manganese-containing binary alloy, with the austenitic matrix and visible dark phases of martensite. This is supported by literature, by Changjiang et al.[7] and Peifeng et al.[8], wrote that Mn addition of greater than 18 wt% promotes the formation of anti-ferromagnetic phases such as  $\gamma$  - austenite or  $\epsilon$  – martensite, these are the phases observed on the A1 and A2 specimens. XRD results also support this with peaks matching the respective phases. It was visually observed, given the same magnification of observation that the amount of the martensite in A2 is less as compared to A1.

The microstructures of the HR specimens are shown in Figure 5, Reference (left), A1 (right) and A2 (bottom). The three micrographs clearly showed the horizontal lines running through from side to side. These specimens were taken parallel to the rolling direction. This directionality is due to the thermomechanical processing the specimens went through before the water-quenching step. The Reference (Figure 5, left) specimen consisted of a martensitic matrix (brown) and visible retained austenite (light areas) along the rolling lines. In the literature, it is shown that martensite and retained austenite are phases observed after heat treatment in this composition [4,6]. A1 (Figure 5, centre) and A2 (Figure 5, bottom) consisted of an austenitic matrix and deformation twins. This is consistent with the observations in the literature [9, 10]. XRD phase analysis also agrees with the observed microstructures, see Figure 6.

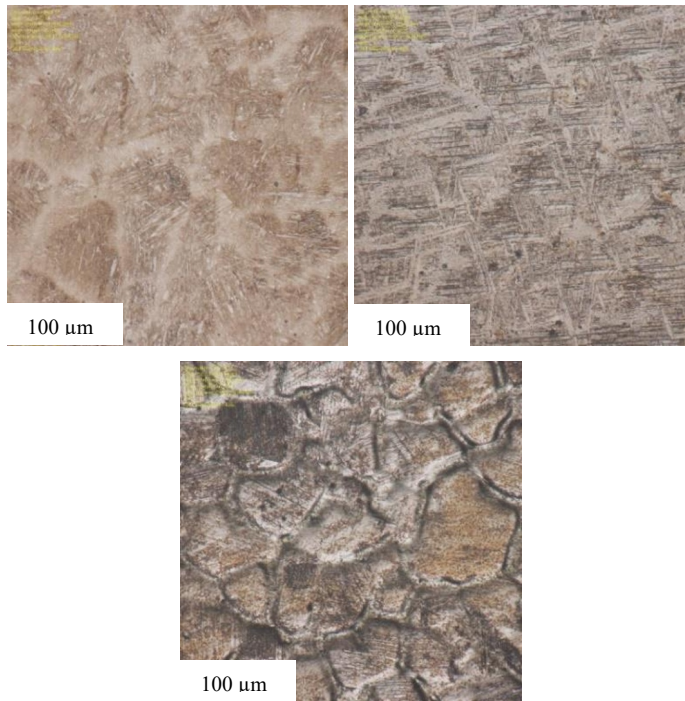


**Fig. 4.** Microstructure of as-cast Reference (left), A1 (right) and A2 (bottom) specimens.

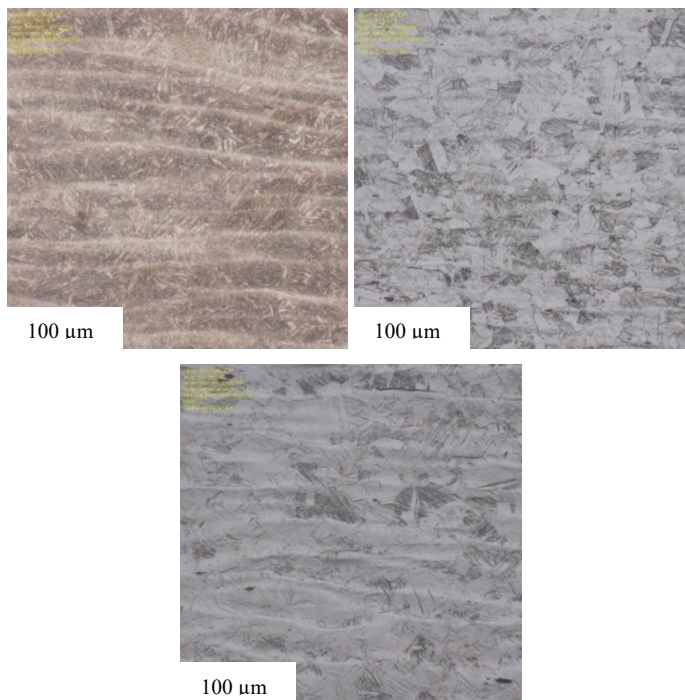


**Fig. 5.** Microstructure of HR Reference (left), A1 (right) and A2 (bottom) specimens.

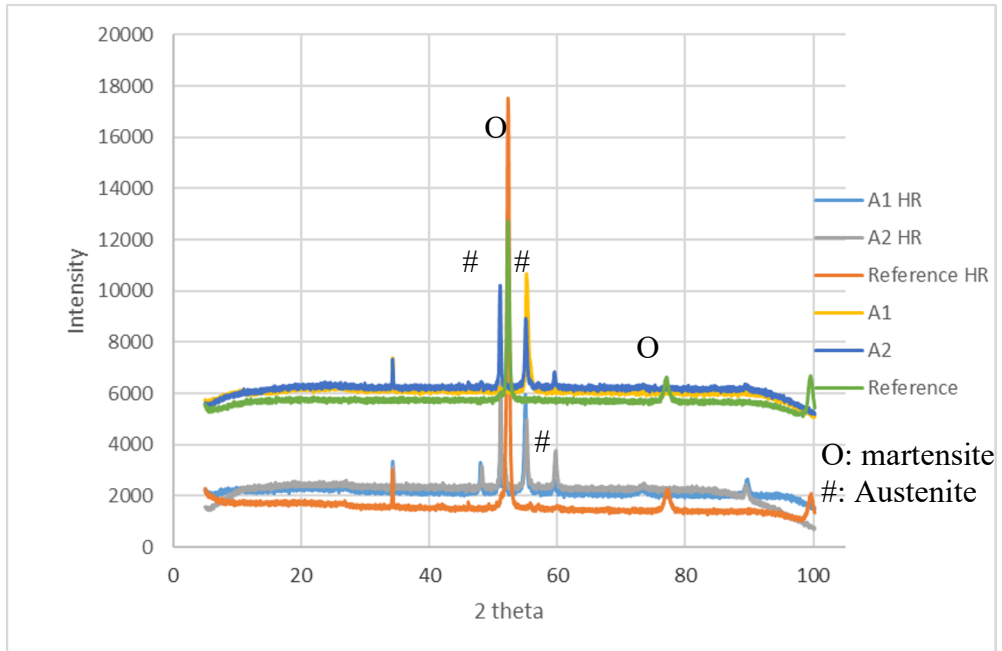


**Fig. 6.** XRD results for as cast and HR Reference, A1 and A2 in the  $2\theta$  range of  $0^\circ$  and  $90^\circ$ .

### 3.2 Hardness

The hardness for the Reference, A1 and A2 specimens were taken at random on the polished surface at an average of 6 indents per sample and the results are shown in Figure 7 Below. The hardness of the Reference specimen was  $407 \pm 17 \text{HV}_{10}$  in the as-cast condition and was 5% more after the HR process. This seems to be minimal change. This hardness is in agreement with the microstructure observed. The as-cast hardness for A1 was  $208 \pm 7 \text{HV}_{10}$  and increased by 9%. A2 hardness was  $217 \pm 14 \text{HV}_{10}$  as cast and was 6% less after the HR process. There is a noticeable hardness difference observed between the Reference, A1 and A2 specimens, The reference is almost two times the hardness of both A1 and A2 in both conditions of as cast and HR process.

Since this is preliminary work, tests such as Tensile, Charpy impact test and heat treatment will be conducted on all the alloys in the near future.

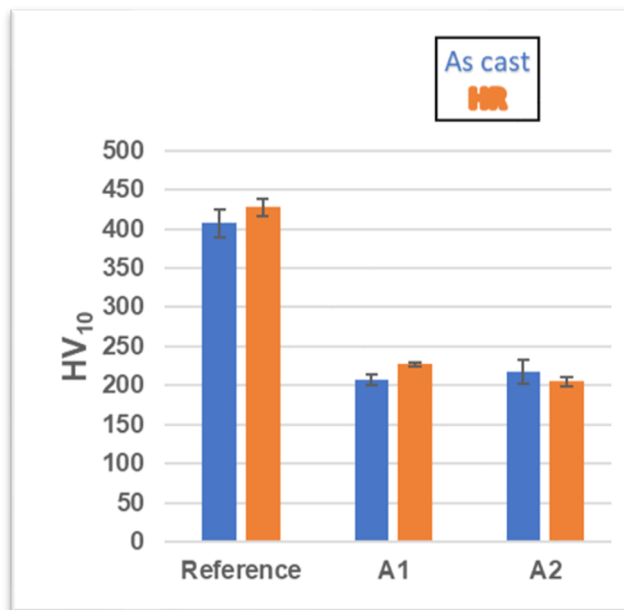


**Fig. 7.** Vickers hardness of as-cast and HR 9%Ni reference and the two FeMn binary compositions (A1 and A2).

## 4 Conclusion

The microstructure of the reference for both conditions was of martensite with retained austenite, as such higher hardness was obtained. The hardness for A1 and A2 specimens was not different, with their difference being below 10% which was consistent with the austenitic microstructure obtained. The hardness of the reference was almost 50% higher than that of A1 and A2. XRD results are in agreement with the observed microstructure and the phases in the literature.

The authors extend their sincere appreciation to MINTEK and the Department of Science and Innovation's Advanced Metals Initiative (AMI) for their generous financial support.

## References

1. K. Hickmann, A. Kern, U Schriever, J. Stumpfe, ThyssenKrupp Stahl AG, Division Metallurgy/Heavy Plate, Profit Center Heavy Plate, Germany
2. K. Jisun, K. Jaewoong, P. Changmin C, Kwangsan, MDPI, (2021)
3. 9% Nickel Steel for LNG and Cryogenic Applications. Available at: <https://masteel.co.uk/news/9-nickel-steel-lng-cryogenic-applications> (Accessed on 04/04/24)
4. 9% Nickel Steel, Available at: <http://www.metalspiping.com/9-nickel-steel> (Accessed on 04/04/24)

5. N. Fakude, South Africa Critical Minerals, African Critical Minerals Summit 29 August 2023, Available at: <https://www.mineralscouncil.org.za/search-results?q=african+critical+minerals> (Accessed on 05/04/2024)
6. Y. Tomota, M. Strum, J. Morris, W, Jr., Metall. Trans. A, Volume 17A, (1986)
7. S. Changjiang, X Wenbin, Z. Jun, Gu Yuanyi., Z. Qijie, Mat. and Des., Volume 51, 262–267, (2013)
8. L. Peifeng, W. Hong, L. Luxin, S. Deye, L. Jingbo, M. Xueru, L. Kaiyang, F. Qihong, T. Yingtao, I. Baker, Mat. Sci. & Eng. A 852, 143585, (2022)
9. Z.G. Liu, X.H. Gao, M. Xiong, P. Li, R.D.K. Misra, D.Y. Rao, Y.C. Wang, Mat. Sci. & Eng. A 807, 140881, (2021)
10. G. Adam, K. Aleksandra, G. Barbara, Metals., 8, 122; doi:10.3390/met8020122, (2018)